

Development of Commercial Grade Silicon Drift Detector with On-Chip JFET: Device Design, Technology & Characterization

Dr. Paurus Mehta ¹ and Dr. Paurus Mehta ²

¹ Bhabha Atomic Research Centre

Received: 7 February 2012 Accepted: 3 March 2012 Published: 15 March 2012

Abstract

Proto-type Silicon Drift Detectors (SDDs) Proto-type Silicon Drift Detectors (SDDs) have been realized through a pilot stage fabrication run at the Micro-fabrication facility at Indian Institute of Technology - Bombay (IIT-B). Taking precedence from the fabrication run at IIT-B, commercial grade SDDs with on-chip low noise JFETs are being developed for low energy X-ray spectroscopy and position sensing applications using silicon bipolar technology available with Bharat Electronics Ltd (BEL), Bangalore. This paper presents a detailed illustrative view on the design; fabrication and characterization of the SDDs in-built JFETs fabricated at BEL. Traditionally, detectors are fabricated over high resistivity silicon substrates whereas JFETs are fabricated over low-resistivity silicon. To design a process for fabrication of both SDD and JFET over high resistivity silicon posed a sufficient technological challenge. Simulations in Technology Computer Aided Design (TCAD) proved helpful in arriving at optimum process parameter values for fabrication of SDDs and on-chip JFETs over the same high resistivity silicon substrate. SDDs low noise JFETs fabricated at BEL were characterized to extract dc (I-V) performance parameters like total leakage current at anode, transconductance etc. These results formed precursors to fine-tuning the process for the next run aimed at achieving an even lower leakage current level.

Index terms— Silicon Drift Detector, Junction Field Effect Transistor,

1 Introduction

ilicon drift detector (SDD) is a device based on the principle of lateral charge transport within the bulk of a fully depleted detector, as proposed by Gatti and Rehak (Reference-1). SDD is essentially detector in which a high resistivity n-type silicon substrate is employed to fabricate p-n junctions on both sides of the substrate. PN junctions on the front side form segmented field shaping cathodes whereas a uniform, p-n junction forms the back-cathode. A reverse bias gradient when applied to the field shaping cathodes together with a constant back-contact voltage creates a potential distribution in the shape of a "Potential Gutter" with the ultimate electron potential energy minimum at the anode. Electron-hole pairs created by passage of ionizing radiation are swept vertically by the parabolic potential along the depth and focused at the local potential minima from where they get drifted along the lateral drift channel towards the anode. The distinguishing feature of the SDD is that its small output (anode) capacitance is independent of its large detector active area.

Thus SDDs are suitable for high resolution (127eV @ 5.9 keV for Mn-K[?] line; Ketek Vitus SDD) and high count rate (~1x10⁶ cps) X-ray spectroscopy applications. These detectors have found wide application in high-energy physics for tracking applications. SDDs have been incorporated in the ALICE detector along the Large Hadron Collider at CERN. This high-resolution capability of SDDs can be further augmented by integrating the input device of the pre-amplifier (JFET) with the detector so as to avoid stray capacitance and microphonism arising

42 due to wire bonding between them. The integration of JFET onto the detector also facilitates better matching
43 between detector and transistor capacitances.

44 The proto-typing stage fabrication of SDDs at IIT-B has been successfully completed. The first run of the
45 fabrication of the commercial grade SDDs and JFETs has yielded satisfactorily good results. SDDs fabricated
46 at BEL were aimed at both Xray Spectroscopy and position sensing applications. Circular geometry SDDs
47 with in-built low noise JFETs were designed for X-ray Spectroscopy applications. Linear geometry SDDs
48 with on-chip poly-silicon resistors were designed for 1D & 2D position sensing applications. Additionally, high
49 transconductance JFETs were also designed together with various different kinds of SDDs over the 4-inch silicon
50 wafer.

51 2 II.

52 3 Detector Design

53 This particular version of SDD has an on-chip Poly-Resistor network for biasing the intermediate p+ strips
54 together with an on-chip JFET for first level amplification [Fig. ??(b)]. The anode is in geometry of an annular
55 ring having 50 μm radii with an area of $7.7 \times 10^4 \mu\text{m}^2$ that fetched an analytical full depletion capacitance
56 of 27 fF for 300 μm thick fully depleted silicon wafer. The total active area of the detector was $2.31 \times 10^7 \mu\text{m}^2$.
57 This device had 20 p+ strips with two guard rings encircling its outer perimeter. The first, fifth, tenth,
58 fifteenth, twentieth, and last p+ strips were individually biased whereas the of rest p+ strips got biased by the
59 on-chip resistor. Each poly resistor was designed to present a Fig. 1 (a) : Composite layout of Circular SDD
60 (Pitch-120 μm) with in-built JFET. On the basis of the success of the fabrication effort at IIT-B, the process for
61 the BEL effort was formulated. Formulation of a process for fabrication of SDD and JFET over high resistivity
62 silicon substrate was a significant technological challenge. The process for the fabrication of SDD with integrated
63 JFET was formulated with a view of achieving a high breakdown voltage of >100V, and achieving as low leakage
64 current as possible using the existing fabrication setup at BEL. The process employed at BEL involved all the
65 standard unit processes like oxidation, lithography, etching, and implantation, metallization etc. employed in a
66 bipolar fabrication line. The process parameters have been fine tuned and frozen after a thorough TCAD process
67 simulation study in order to achieve the desired doping profiles for both SDD & JFET. The highest standards of
68 cleanliness and care in planning the unit processes have been maintained to achieve the objectives of low leakage
69 currents together with admissibly high breakdown voltages. Moreover, the process had to be compliant with the
70 technological constraints of the BEL foundry. Additionally, Polysilicon process has been employed for fabrication
71 of on-chip resistor network. The distinguishing feature of this process was the employment of a double-sided
72 processing for back to front alignment of cathode implants. Thus making double sided SDDs a reality, which
73 are far more superior to single sided SDDs. The lithographic quality was again a challenge as the fabrication
74 process involved 14 lithographic steps. definition of the p-type isolation well (Mask-1) within the center of the
75 SDD for housing the embedded JFET. This was followed by an oxide etch step to expose the substrate for boron
76 implantation ($E = 80 \text{ keV}$; Dose = $5 \times 10^{11} \text{ cm}^{-2}$). Subsequent dopant activation and drive-in diffusion of
77 boron species was performed employing the Drive-in cycle as illustrated in the Fig. 4. The simulated doping
78 profile for the p-well implant showed a peak boron concentration of $3.39 \times 10^{14} \text{ cm}^{-3}$ for a junction depth of
79 3.19 μm and an extracted sheet resistance of 102.705 $\text{k}\Omega/\square$. Subsequently, the n-channel within the p-well region
80 was lithographically defined (Mask-2) and phosphorus implantation ($E = 150 \text{ keV}$; Dose = $5 \times 10^{12} \text{ cm}^{-2}$) was
81 performed followed by a drive-in cycle (Fig. ??) to form the n-channel. The simulated doping profile (Fig. 7)
82 for the n-channel showed a peak phosphorus concentration of $3.24 \times 10^{16} \text{ cm}^{-3}$ for a junction depth of 2 μm and an
83 extracted sheet resistance of 2.703 $\text{k}\Omega/\square$.

84 Going ahead from here, the p+ cathodes & p+ guard ring (Mask-3) were lithographically defined on the
85 topsurface whereas the p+ backcontact (Mask-4) was defined on the bottom surface of the wafer employing back
86 to front double-sided alignment lithography. A thin screen-oxide (Fig. ??) was grown over the exposed silicon
87 to create shallow junctions and prevent implantation damage. Boron Implantation (Dose = $1 \times 10^{15} \text{ cm}^{-2}$; Energy
88 = 80 keV) followed by dopant activation and drive-in (Fig. ??) was performed to create p+ strips, p+ guard ring
89 and p+ back-contact regions. The simulated doping profile showed a peak boron concentration of $2.24 \times 10^{18} \text{ cm}^{-3}$
90 for a junction depth of 1.5 μm and extracted sheet resistance of 181.93 $\text{k}\Omega/\square$. The 5th lithographic (Mask-5)
91 step was performed for definition of p+ type Gate region of the JFET. Boron Implantation (Dose = $1 \times 10^{15} \text{ cm}^{-2}$;
92 $E = 80 \text{ keV}$), followed by Drive-in (Fig. 12) was performed to realize the p+ gate region. In the p+ Gate
93 Drive-in case, the analytical value of sheet resistance was 181.93 $\text{k}\Omega/\square$, for a junction depth of 1.1 micron and the
94 extracted peak Boron concentration of $1 \times 10^{19} \text{ cm}^{-3}$. Subsequently, n+ Anode, Source & Drain were defined
95 (Mask-6) followed by Phosphorus Implantation (Dose = $1 \times 10^{15} \text{ cm}^{-2}$; $E = 80 \text{ keV}$) forms the n+ regions.
96 The dopant activation and drive-in was performed as per schedule in figure 14. The simulated analytical sheet
97 resistance was 79.3 $\text{k}\Omega/\square$, for a characteristic depth of micron and the extracted peak Phosphorus concentration
98 was $1.1 \times 10^{20} \text{ cm}^{-3}$. Following this, oxide openings (Poly-contact: Mask-7) were defined over the p+ strips
99 region to facilitate the poly-silicon layer deposited in the next step to make contact with under-lying p+ region.
100 Poly-Silicon was then deposited and boron implantation was performed to form the poly-resistors having a Sheet
101 Resistance of 138.88 $\text{k}\Omega/\square$. After lithographically patterning (Mask-8) the polysilicon layer a short anneal step
102 (Time = 30 minutes; Temperature = 900 o C) was carried out to dopant activation of the species in the poly

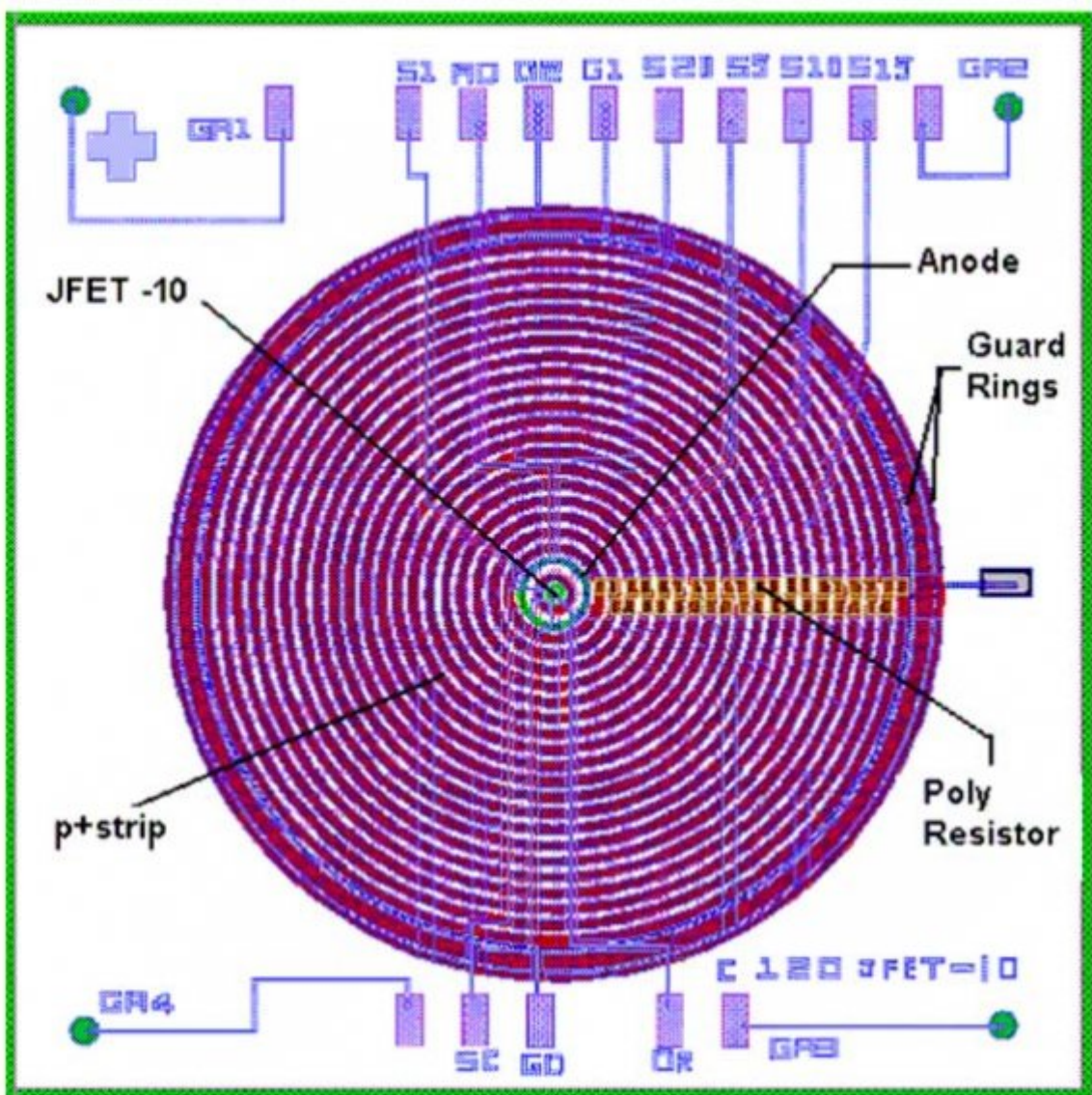
103 layer. Proceeding from that, the contact lithography (Mask-9) was performed to open windows through the oxide
 104 for making contact with Aluminum metal deposited above for purpose of electrical connection with rest of the
 105 electronics. The back-contact was defined (Mask-10) for contact window openings on the back surface of the
 106 wafer. Aluminum metallization (Thickness = 1.5 microns) was carried out over the front-surface and lithography
 107 was performed (Mask-11) to pattern the metal layer to define the various electrical connections. The back-
 108 side was then metalized keeping the front surface protected and the metal layer was patterned lithographically
 109 (Mask-12) to form the backelectrodes of the SDD. Lastly, Protective glass was deposited over both the front and
 110 back-sides followed by lithography (Masks-13 & 14) to open areas over the metal bond pads. The values for
 111 sheet resistances, junction depths for various regions have been tabulated in Table ?? process. I-V was taken by
 112 ramping the voltage at the strip (Cathode-6) from -100 V to 0 V and the anode current was measured through an
 113 ammeter (Keithley-2400 SMU used in current sense mode). I-V characteristics were measured for various values
 114 of guard-ring voltages (illustrated in Fig. 15). The nature of the I-V curve matched with the nature of I-V curve
 115 achieved for the SDDs in IIT case. The embedded lownoise JFET was characterized for its dc performance using
 the same experimental setup. 1. ? ? ? ? ? ? (?/)¹



Figure 1: Fig. 1 (

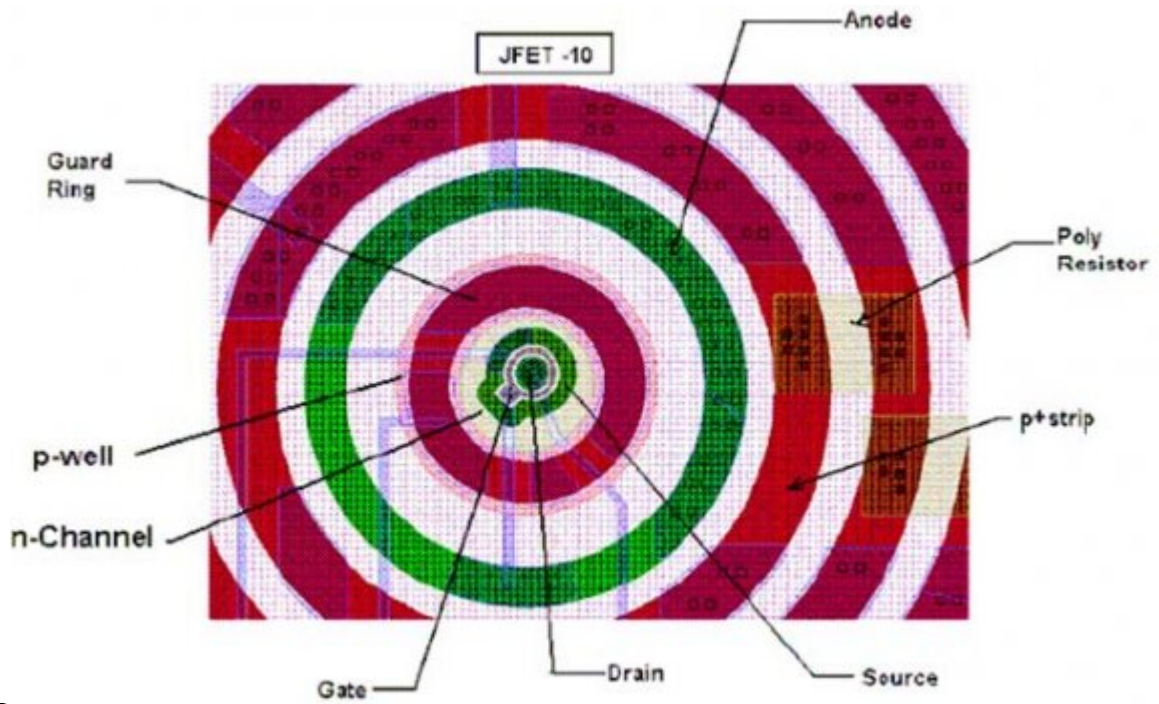
116

¹© 2012 Global Journals Inc. (US)



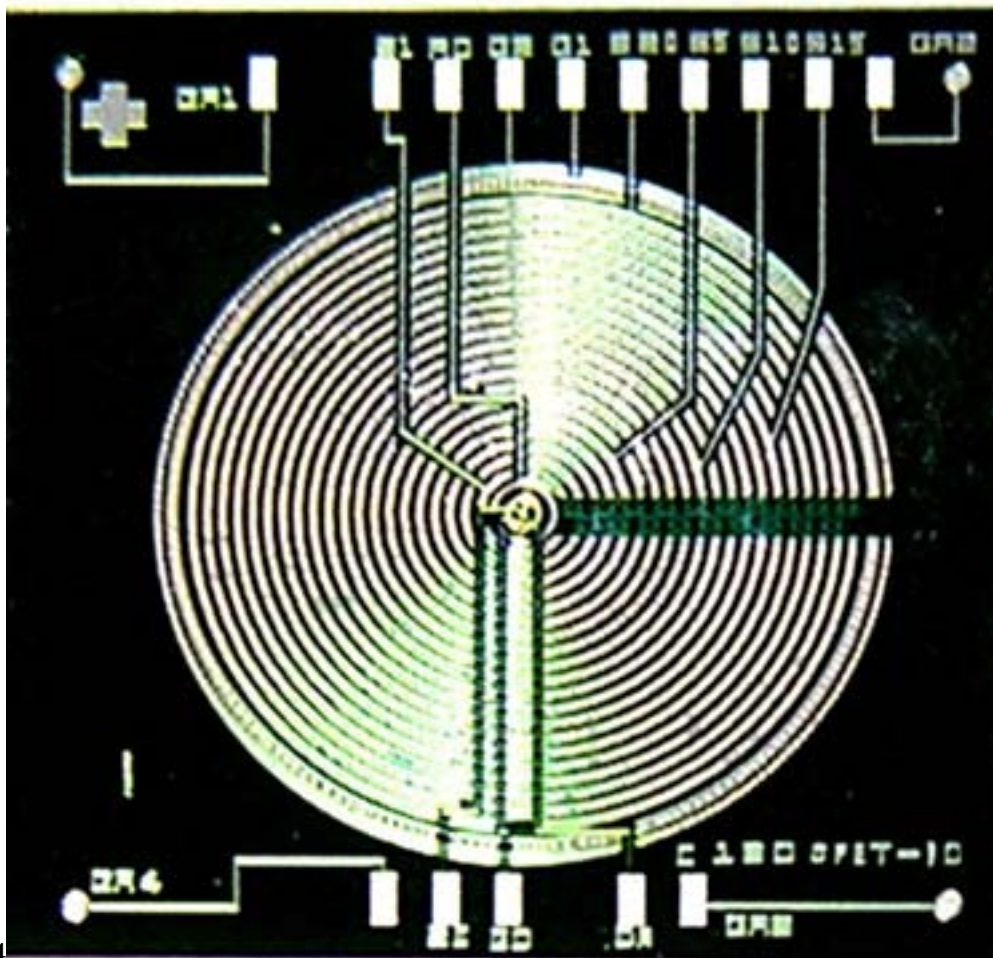
1

Figure 2: ?Fig. 1 (



23

Figure 3: Fig. 2 :Fig. 3 :



4

Figure 4: Fig. 4 :

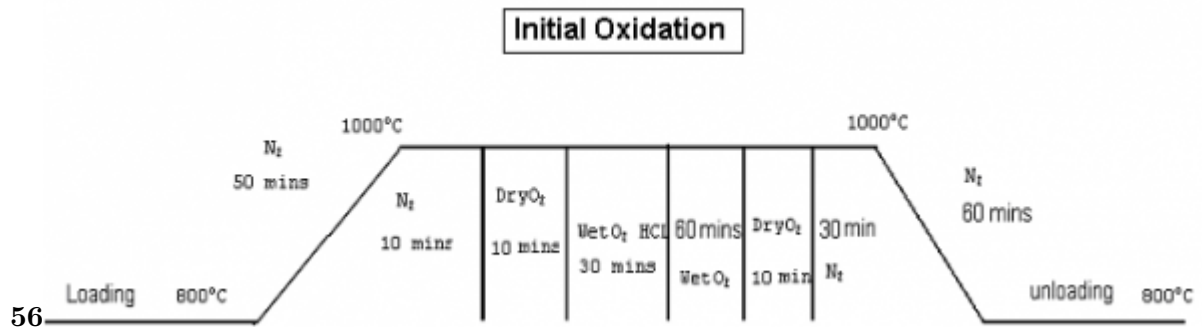


Figure 5: Fig. 5 :Fig. 6 :

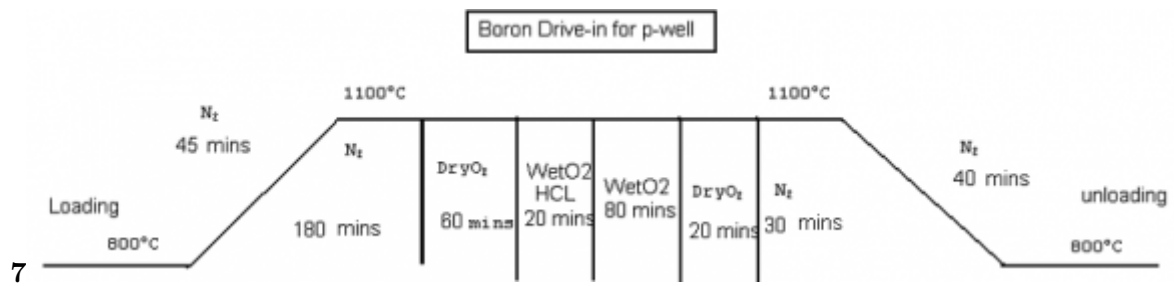
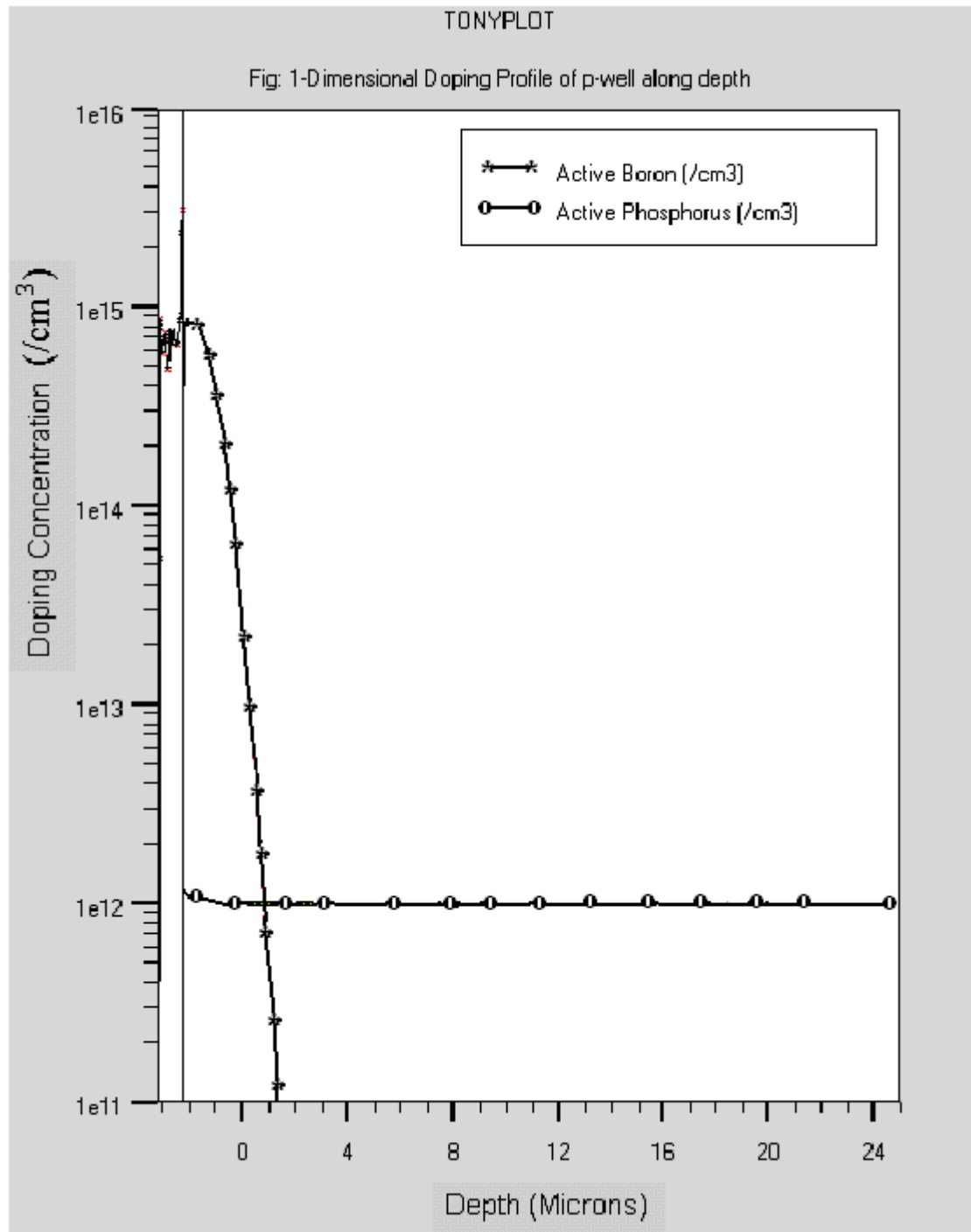
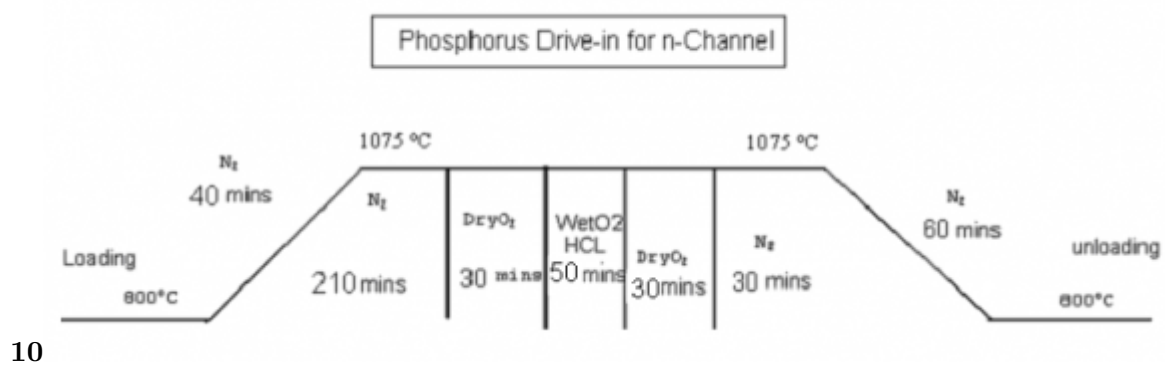


Figure 6: Fig. 7 :



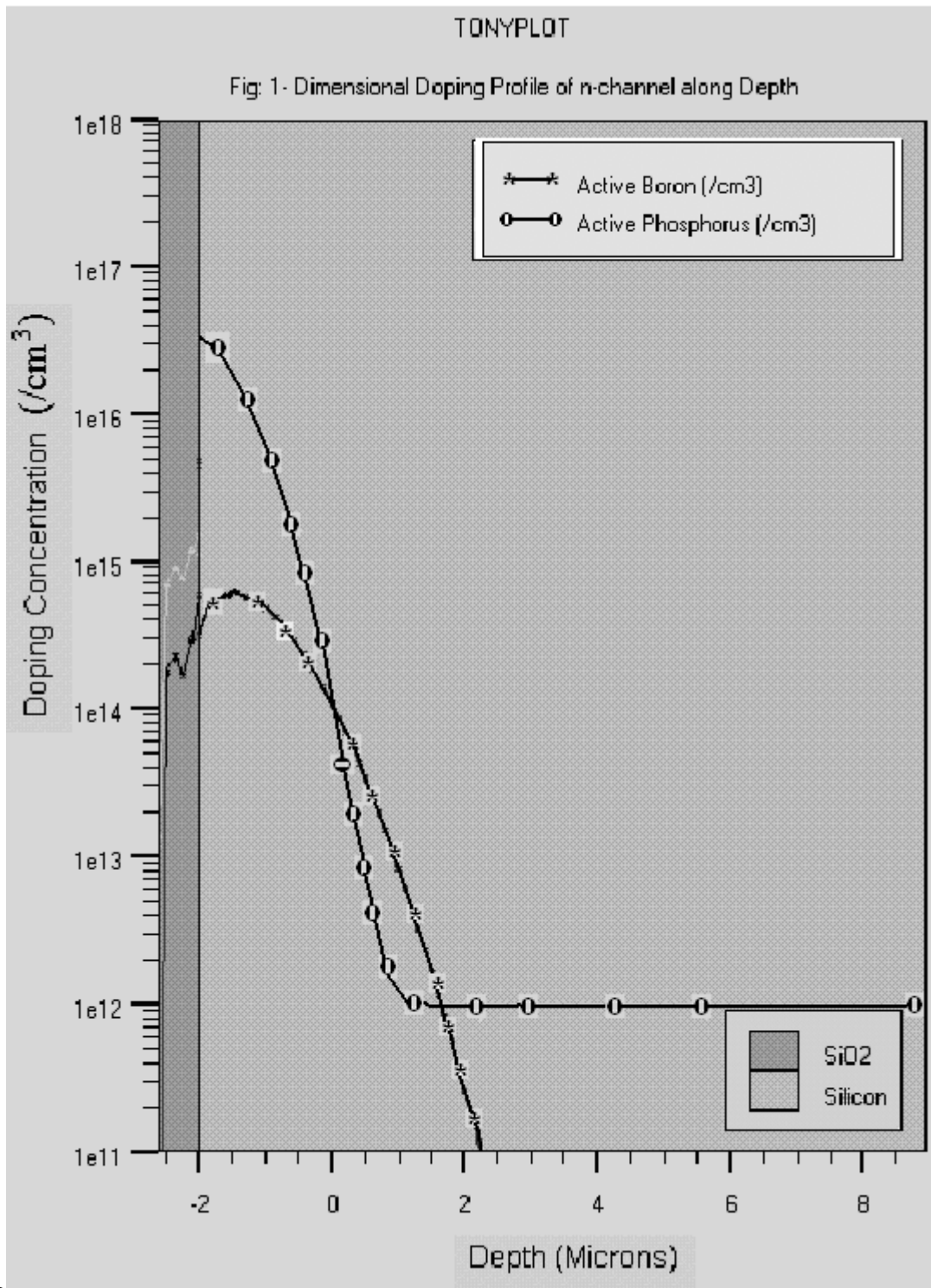
89

Figure 7: Fig. 8 :Fig. 9 :



10

Figure 8: Fig. 10 :



12

Figure 9: Fig. 12 :

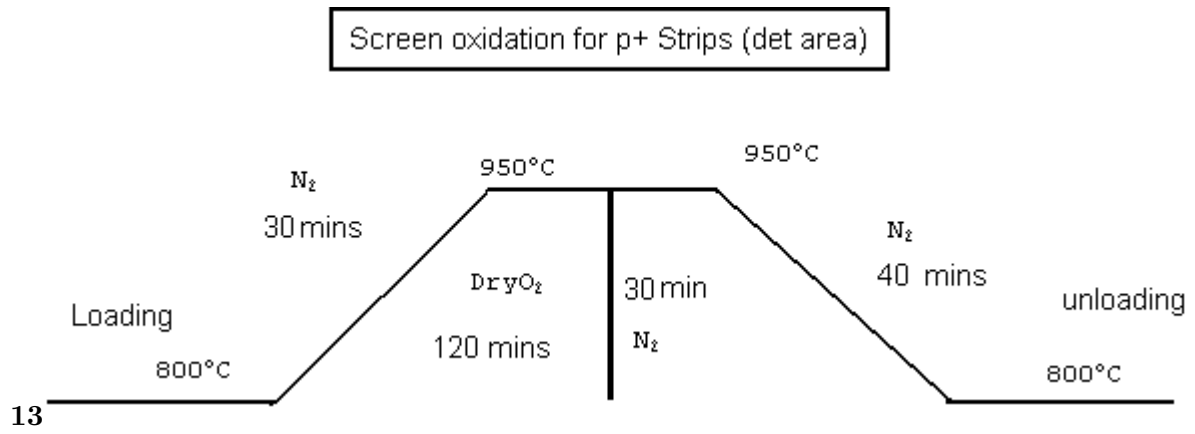


Figure 10: Fig. 13 :

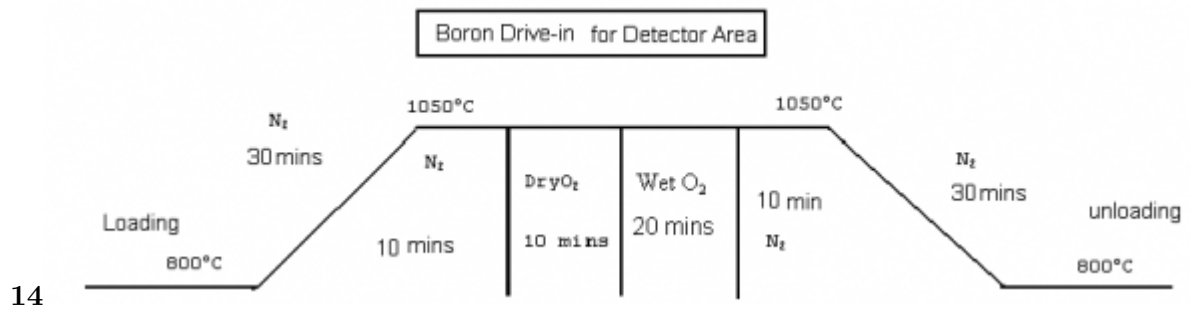
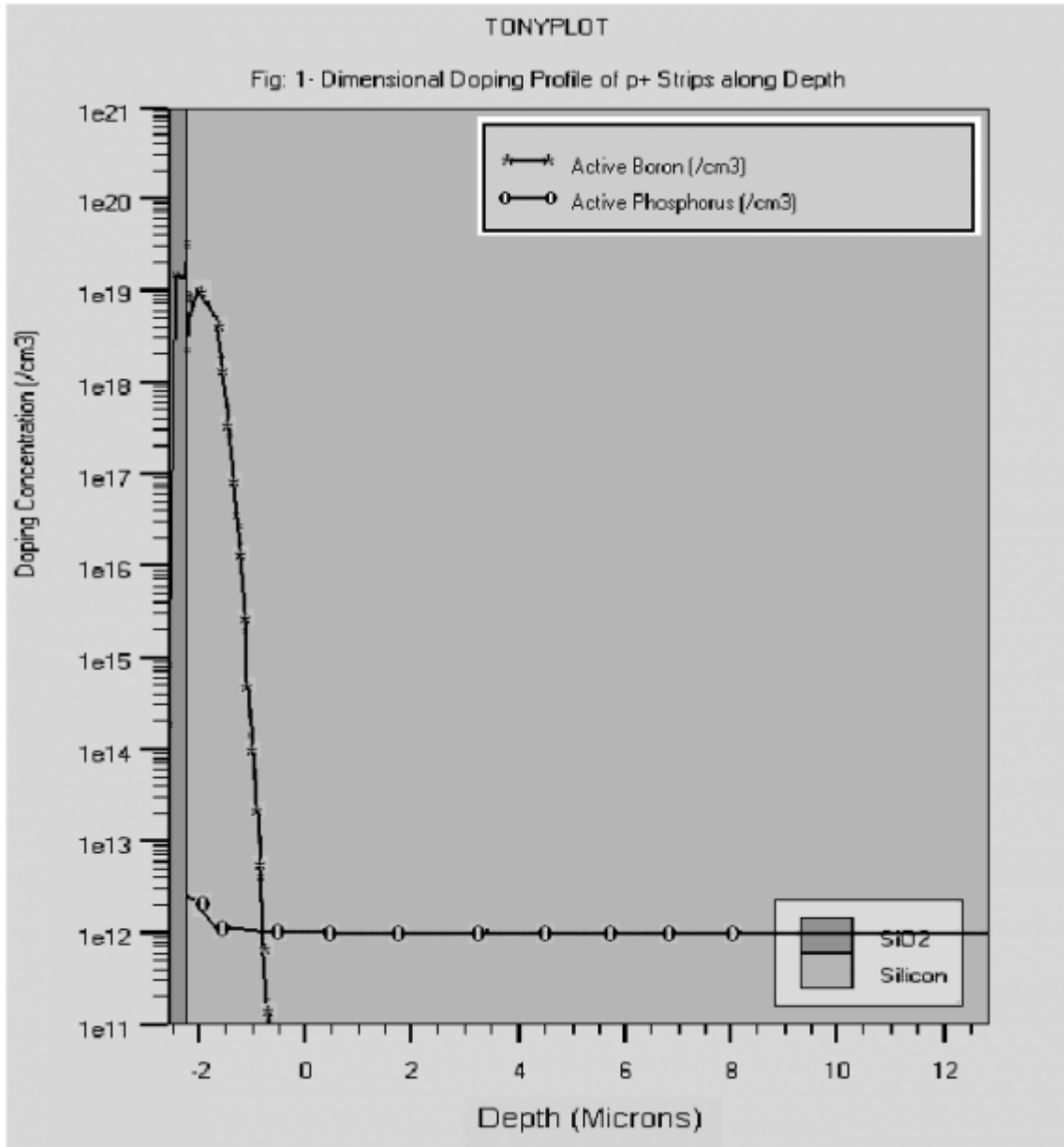


Figure 11: Fig. 14 :p



1516

Figure 12: Fig. 15 :Fig. 16 :

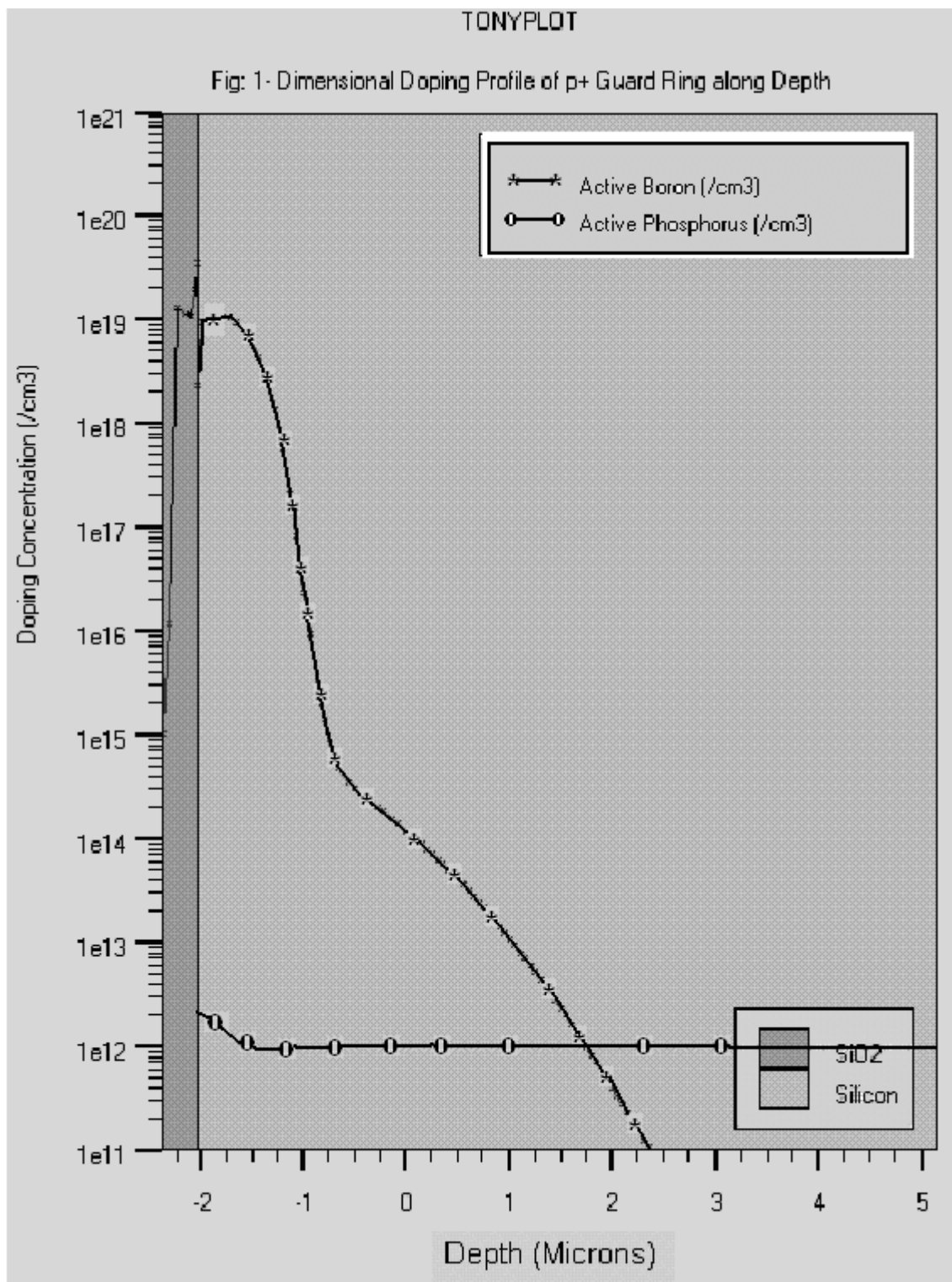


Figure 13:

11

Figure 14: 1 Table 1 :

117 .1 Acknowledgements

118 The author expresses a deep sense of gratitude for Late Dr. S. K. Kataria for his guidance and leadership. The
119 author would like to especially thank Mr. G. P. Srivastava, Mr. Shekhar Basu and Dr. Sinha for their kind
120 support. deviation of less than 30% from that achieved from characterization. The value of noise figure (5.69
121 nV \sqrt Hz) was within the low noise band.

122 V_{GS} = 0 Volts V_{GS} = -0.25 Volts V_{GS} = -0.5 Volts V_{GS} = -0.75 Volts
123 2.0x10

124 [Gatti and Rehak ()] , E Gatti , P Rehak . *Nucl. Instrum. Meth. A* 1984. 225 p. 608.

125 [Lechner et al. ()] , P Lechner , C Fiorini , R Hartmann , J Kemmer . *Nucl. Instr. & Meth. A* 2001. 458 p. 281.

126 [Rashevsky et al. ()] , A Rashevsky , V Bonvicini , P Burger , S Piano , C Piemonte , A Vacchi . *Nucl. Instr. &*
127 *Meth. A* 2002. 485 p. 54.

128 [Mehta et al. ()] ‘Silicon drift detectors with integrated JFET: Simulation and design’. P Mehta , V & S K Mishra
129 , Kataria . *Indian Journal of Pure and Applied Physics* 2005. 43 p. 705.

130 [Mehta and Sudheer ()] ‘Studies of the Silicon Drift Detector: Design, Technology Development, Characteriza-
131 tion & Physics Simulations’. Pourus Mehta , * Sudheer , KM . *Armenian Journal of Physics* 2011. 4 p.

132 .